Anisotropic lattice expansion determined during flash sintering of $BiFeO_3$ by in-situ energy-dispersive X-ray diffraction

Mary Anne B. Wassel[a*], Luis A. Pérez-Maqueda[b], Eva Gil-Gonzalez[bc*], Harry Charalambous[a], Antonio Perejon[bd], Shikhar K. Jha[a], John Okasinski[e], Thomas Tsakalakos[a]

[a]Department of Materials Science and Engineering, Rutgers University, 607 Taylor Road, Piscataway, NJ 08854, United States

[b]Instituto de Ciencia de Materiales de Sevilla, Consejo Superior de Investigaciones Científicas−Universidad de Sevilla. Calle Américo Vespucio 49, Sevilla 41092, Spain

[c]John A. Paulson School of Engineering and Applied Sciences, Harvard University, Cambridge, Massachusetts 02138, United States

[d]Universidad de Sevilla, Departamento de Química Inorgánica, Facultad de Química, Universidad de Sevilla, Sevilla 41071, Spain

[e]X-Ray Science Division, Advanced Photon Source, Argonne National Laboratory, Argonne, Illinois 60439, United States

Corresponding authors: Eva Gil-Gonzalez: eva.gil@icmse.csic.es and Mary Anne Wassel, mab.wassel@gmail.com

Keywords: sintering, energy dispersive X-ray diffraction, $BiFeO_3$, nanocrystalline materials

Abstract

$BiFeO_3$ has a Curie temperature (T_C) of 825°C, making it difficult to sinter using typical methods while maintaining the purity of the material, as unavoidably secondary phases appear at temperatures above T_c. Flash sintering is a relatively new technique that saves time and energy compared to other sintering methods. $BiFeO_3$ was flash sintered at 500°C to achieve 90% densification. In-situ energy dispersive X-ray diffraction (EDXRD) revealed that the material did not undergo any phase transformation, having been sintered well below the T_C. Interestingly, anisotropic lattice expansion in the material was observed when the sample was exposed to the electric field.

$BiFeO_3$ is a perovskite-type material that has unique multiferroic properties at room temperature [1, 2]. Applications for $BiFeO_3$ include ferroelectric memory devices and a potential piezoelectric replacement for lead-based materials like PZT [3, 4]. However, as a complex oxide with low thermal stability, $BiFeO_3$ is difficult to process under conventional sintering conditions since dense pellets require high temperature for long periods of time which result in decomposition and/or the appearance of secondary phases.

Having rhomobohedral structure at room temperature, the hexagonal lattice parameters are a=5.58 Å and c=13.90 Å [3]. The linear thermal expansion coefficients based on a hexagonal formulation vary depending on temperature, and this relationship was first determined by Bucci et al [5, 6].

Since conventional methods require large amounts of energy and time, field assisted sintering techniques (FAST) have been developed [7, 8]. Flash sintering is a relatively new FAST technique [9-14]: Cologna, et al. published the first paper in 2010 [11]. They sintered nanograin zirconia at 850°C in less than 5 seconds, much lower than the typical conditions for conventional sintering [11]. The technique is similar to spark plasma sintering (SPS), but in this case the current passes through the sample and the electrical requirements become dependent on the material's response to the applied electric field. Insulator ceramics typically need a higher electric field to flash [15]. Flash sintering can be described in three stages, which has been detailed by Jha et al. while working on isothermal conditions [16].

Since Cologna's work, flash sintering has been investigated for a variety of oxide, non-oxide, and composite materials under both AC and DC fields [17, 18].

However, there has been much disagreement regarding the possible mechanisms for flash sintering. Arguments have been made for the local heating of grain boundaries, the nucleation of avalanches of lattice defects, and thermal runaway [19-23], but none have gained widespread acceptance.

Different techniques have been used to study the effect of electric field on sintering [24-31]. X-ray diffraction is one of the best-known techniques for understanding possible changes in structure during processing. But in a typical lab x-ray diffraction setup, the beam energy is not enough to penetrate bulk materials, and the beam intensity does not allow for very rapid data acquisition.

Energy dispersive X-ray diffraction (EDXRD) differs from traditional XRD in that the angle of the detector is kept constant and a wide range of X-ray wavelengths pass through the sample. This allows for diffraction data to be acquired for all relevant crystal faces simultaneously. Moreover, the intensity of the X-rays is very high allowing a deep penetration through solids and quicker data acquisition.

Previous work has been done on the flash sintering of $BiFeO_3$ and the reactive flash sintering of $BiFeO_3$ [32, 33]. It was shown that densification occurred with low porosity while retaining the purity and the insulating nature of the samples. It was proposed that electric current plays some role in enabling the sintering process. Conversely, it has been demonstrated that spark plasma sintering adversely impacted the electrical properties of the material, which exhibited high conductivity due to the reducing conditions used in this technique [34-36].

The aim of this work is to gain more understanding of how $BiFeO_3$ is affected by the electric field and current during flash sintering. In-situ EDXRD was used for this purpose.

The $BiFeO_3$ powders were prepared via direct mechanosynthesis following the procedure presented in Ref [37]. Green bodies 5 mm in diameter and 5 mm thick were compacted uniaxially with cylindrical dies to achieve approximately 50% of the theoretical density.

High energy dispersive x-ray diffraction (EDXRD) was used *in-situ* at the synchrotron facility at Argonne National Laboratory. The employed 6 BM-A beamline delivers photons with energies up to 200 keV. The EDXRD setup is shown in Figures 1a-b. Thus, the sintering behavior was studied *in-situ* since the penetration depth is large enough for the beam to pass through the furnace, which allows for tracking phase transformations and the temperature of the specimen. This information can be analyzed and used to explain general flash sintering phenomena, which will help resolve diverging theories.

The governing equations for EDXRD are Bragg's Law,

$$n\lambda = 2d_{hkl}\sin\theta$$

where $n =$ a positive integer, $\lambda =$ wavelength, $d_{hkl} =$ the interplanar spacing of the (hkl) reflection in Angstroms, and $\theta =$ the detector angle, and Planck's equation,

$$E = hv$$

where $E =$ energy in eV, $h =$ Planck's constant $= 4.135 \times 10^{-35}$ eV, $v =$ frequency $= c/\lambda$ (where $c =$ speed of light $= 2.9979 \times 10^{8}$ m/s). Solving both equations for wavelength, and substituting constant values, we have an equation for the scattered energy of the (hkl) reflection in keV as a function of interplanar spacing:

$$E_{hkl} = \frac{6.199}{d_{hkl}\sin\theta} \qquad (1)$$

A white x-ray beam is generated and passes through the sample gauge volume (shown in yellow in Figure 1a), whose position is controlled by a three-axis sample stage. The gauge volume is a parallelepiped whose size is dependent on the size of the incident beam collimation slits and the Bragg angle. The diffracted beam is recorded at a fixed Bragg angle 2θ=3° (Figure 1b). Higher Bragg angles reduce the intensity of the beam.

Custom furnaces that reach up to 1150°C were developed for the *in-situ* experiments. The pellets were coated on top and bottom with a platinum paste that function as electrodes. The heating coils of the furnace have a separate power supply (BK Precision 9115 DC) which was turned on to increase the furnace temperature, with a feedback system of a K-type thermocouple placed close to the sample. When the desired temperature was reached during an isothermal experiment, an electric field was applied through the electrodes to the sample, controlled by a BK Precision PVS DC power supply (Furnace setup detailed in Figures 1c-d).

The interplanar spacing for the (104) and (110) reflections of $BiFeO_3$ were identified using the ICDD standard for $BiFeO_3$ [38]. The peak breadth was determined by manually identifying the peaks and fitting them with a Gaussian function using Fityk [39].

A MATLAB program to complete a pseudo-Voigt fit was developed, which converts the channel numbers to energy levels based on calibration data of the beamline, and

specifies the number of peaks to fit. For $BiFeO_3$, where the (104) and (110) peaks are so close together, an initial starting intensity, energy, and FWHM for the (104) peak is input (based on a long scan of the material prior to flash), and the location of the (110) peak is defined in terms of the (104) peak. The accuracy of the fits can be compared based on the starting parameters. Once the energies of the two peaks are fit, the values are superimposed over a waterfall plot to show the change in peak locations during an experiment. These fit energies are used to calculate and graph the interplanar spacings and subsequently the hexagonal lattice parameters.

In this work, a furnace temperature was set to 500°C at a rate of 10 °C/min. Then, a 50 V/cm electric field was applied across the sample, limiting current density to 25 mA/mm^2. One EDXRD profile was taken every three seconds for the duration of sample heating, flash sintering, and sample cooling to monitor and analyze changes in the XRD pattern. Moreover, in another experiment, five-minute EDXRD scans were also taken before and during flash sintering to compare peaks, since this XRD patterns have higher intensity.
A conventional sintering experiment without the application of an electric field was also performed for comparison purposes.
Temperature, electric field, current density, and power density data were synchronized to the EDXRD spectra collected for each experiment. Calculations were completed for determining lattice parameters with respect to time and temperature.

Figure 2a shows the electric field, current density, and power density versus time for the experiment. The incubation, onset, and transient stages of flash are apparent and have been properly marked in Figure 2a. It can be observed that at approximately 111 seconds the power supply switches from voltage to current controlled mode due to the increase of the sample conductivity. At this point, the flash is maintained for thirty seconds.

Figure 2b shows a horizontal waterfall plot of the peak energies with respect to time. The (104) and (110) peaks remain separate, which signifies that a phase transformation from rhombohedral to orthorhombic has not occurred. That is, the sample has remained below the Curie temperature during the flash experiment. Figure 2c shows the corresponding interplanar spacing versus time obtained from Equation (1).

More interestingly, anisotropic lattice expansion is observed when hexagonal lattice parameters are calculated during flash sintering. Figure 3a shows the normalized lattice parameters based on a conventional temperature increase with no application of electric field up to 810ºC. Those parameters increase at a relatively linear rate consistent with the equations developed by Bucci et al [5]. Figure 3b shows the normalized lattice parameters during flash sintering at a furnace temperature of 500ºC, and it is clear that lattice parameter *a* increases much more drastically than *c*. To confirm that this observed anisotropic lattice expansion is not an artifact of the Psuedo-Voight fit, five-minute long scans were taken before flash (to establish peak locations) and during flash. Figure 3c shows that during flash, the diffraction peak corresponding to the (104) plane remains approximately in place while the diffraction peak corresponding to the (110) peak shifts to the left. When the electric field was turned off and the flash event was over the (110) peak recovered its original position, which means that the anisotropic behavior of $BiFeO_3$ during flash is reversible. A similar behavior during flash has been also reported in 3 mol% yttria stabilized zirconia [26]. Additionally, an increase of the relative intensity of the (110)

peak can be observed during flash, which may be attributed to an apparent texturing effect [40].

As it has been mentioned above, Lebrun et al. have experimentally observed anisotropic lattice expansion during flash of 3 mol% yttria stabilized zirconia. From density functional theory, the authors determined the theoretical lattice expansion from the insertion of vacancy-interstitial pairs of oxygen and zirconium, and obtained that the expansion is anisotropic, in agreement with the experimental observation [26]. As an oxide material, an avalanche of Frenkel pairs could be responsible for a similar behavior in $BiFeO_3$. This is not to say that Joule heating does not play some role as well, but it has yet to be determined the exact nature of the relationship that flash sintering has with both Joule heating and large-scale defect generation.

SEM micrographs of the original milled $BiFeO_3$ powder and the densified sample are shown respectively in Figure 4, as well as their corresponding XRD patterns. The microstructure of the milled sample is composed of highly agglomerated particles, which is typical of mechanosynthesized samples (Figure 4a). The X-ray diffraction pattern (Figure 4b) suggests that the sample is pure since all the observed peaks correspond to those of the pure compound, according to the ICCD standard used for $BiFeO_3$ [38]. Moreover, the peaks are broad due to the nanometric character of the crystals. Figure 4c corroborates that densification of 90% as measured by Archimedes method has occurred, presenting nanometric grains, with an average grain size of 60±11 nm. The XRD pattern demonstrates that densification by flash sintering leads to a highly pure sample (Figure 4d), as there is no evidence of peaks associated to secondary phases.

It is of interest to determine the temperature of the sample during flash sintering as this can help determine some of the mechanisms for flash sintering of $BiFeO_3$. However, it is a difficult task. Various groups have used thermocouples, pyrometers, impedance analysis, optical emission spectroscopy, and thermal expansion to estimate temperature with varying success depending on the nature of the error introduced [17].

The black body radiation (BBR) theory is commonly used and assumes that if the sample temperature is initially at the same temperature as the furnace, T_F, and is then electrically heated, the heat dissipation is equivalent to the difference in BBR between the sample and the furnace. The BBR equation for sample temperature, T, is

$$T = T_F \left[1 + \frac{W_V}{\sigma T_F^4}\left(\frac{V}{A}\right)\right]^{1/4}$$

where T_F is the furnace temperature in K, W_V is the power density in $\mathrm{Wm^{-3}}$, σ is the Stefan-Boltzmann constant, $5.67 \times 10^{-8}\ \mathrm{Wm^{-2}K^{-4}}$, V is the volume of the sample in $\mathrm{m^3}$, and A is the surface area of the sample in $\mathrm{m^2}$. Power density was calculated based on the steady state value of the electric field during the transient stage of flash sintering. For the flash sintering experiment at 500ºC, the estimated temperature of the sample is T = 806ºC, and therefore the Curie temperature had not been exceeded, which is in agreement with the EDXRD results (Figure 3c). Moreover, and conversely to the conventionally sintered sample heated up to 810ºC (Figure 3a), it has been observed an anisotropic lattice expansion in that temperature range.

In conclusion, $BiFeO_3$ was successfully flash sintered to high density at a furnace temperature of 500°C. The EDXRD results and the BBR theory suggest that the sample temperature is below the Curie temperature during the flash, which prevents the

decomposition of the sample. Thus, the flash sintered samples are pure and uniformly dense. EDXRD showed an anisotropic lattice expansion of $BiFeO_3$ when exposed to an electric field, inconsistent with pure thermal expansion. The authors believe that a combination of Joule heating and large-scale defect generation are both factors that impact flash sintering, although further work is required to determine the exact nature of these effects. It is clear that EDXRD can play a useful part in determining mechanisms of flash sintering of materials.

This work was supported by the Office of Naval Research (ONR) [N00014-10-1-042, 2010] and [N00014-17-1-2087, Sub 4104-78982, 2017] with Purdue University. Many thanks to Dr. Antti Makinen of ONR for his support and discussions. This research used resources of the Advanced Photon Source, a U.S. Department of Energy Office of Science User Facility operated for the DOE Office of Science by Argonne National Laboratory [DE-AC02-06CH11357, 2006]. EGG thanks Real Colegio Complutense for her grant.

References

[1] J.R. Teague, R. Gerson, W.J. James, Solid State Commun. 8(13) (1970) 1073-1074.
[2] I. Sosnowska, T. Peterlin-Neumaier, E. Steichele, J. Phys. C Solid State 15 (1982) 4835-4846.
[3] G. Catalan, J.F. Scott, Adv. Mater. 21(24) (2009) 2463-2485.
[4] C.R. Bowen, H.A. Kim, P.M. Weaver, S. Dunn, Energy Environ. Sci. 7(1) (2014) 25-44.
[5] J.D. Bucci, B.K. Robertson, W.J. James, J. Appl. Crystallogr. 5 (1972) 187-191.
[6] D.C. Arnold, K.S. Knight, F.D. Morrison, P. Lightfoot, Phys. Rev. Lett. 102(2) (2009) 027602.
[7] C. Ricardo, B. Klaus Van, Sintering: Mechanisms of Convention Nanodensification and Field Assisted Processes, Springer Berlin Heidelberg, Berlin, Heidelberg, 2013.
[8] E. Zapata-Solvas, D. Gomez-Garcia, A. Dominguez-Rodriguez, R.I. Todd, Sci Rep 5 (2015) 8513.
[9] C. Schmerbauch, J. Gonzalez-Julian, R. Röder, C. Ronning, O. Guillon, L. Gauckler, J. Am. Ceram. Soc. 97(6) (2014) 1728-1735.
[10] H. Yoshida, P. Biswas, R. Johnson, M.K. Mohan, J. Am. Ceram. Soc. 100(2) (2017) 554-562.
[11] M. Cologna, B. Rashkova, R. Raj, J. Am. Ceram. Soc. 93(11) (2010) 3556-3559.
[12] S. Grasso, Y. Sakka, N. Rendtorff, C. Hu, G. Maizza, H. Borodianska, O. Vasylkiv, J. Ceram. Soc. Jpn. 119(2) (2011) 144-146.
[13] J.A. Downs, V.M. Sglavo, R. Raj, J. Am. Ceram. Soc. 96(5) (2013) 1342-1344.
[14] A. Gaur, V.M. Sglavo, J. Eur. Ceram. Soc. 34(10) (2014) 2391-2400.
[15] M. Biesuz, V.M. Sglavo, J. Eur. Ceram. Soc. 36(10) (2016) 2535-2542.
[16] S.K. Jha, K. Terauds, J.M. Lebrun, R. Raj, J. Ceram. Soc. Jpn. 124(4) (2016) 283-288.
[17] M. Yu, S. Grasso, R. McKinnon, T. Saunders, M.J. Reece, Adv. Appl. Ceram. 116(1) (2017) 24-60.
[18] C.E.J. Dancer, Mater. Res. Express. 3(10) (2016).
[19] R.I. Todd, E. Zapata-Solvas, R.S. Bonilla, T. Sneddon, P.R. Wilshaw, J. Eur. Ceram. Soc. 35(6) (2015) 1865-1877.
[20] J. Luo, Scripta Mater. 146 (2018) 260-266.
[21] H. Charalambous, S.K. Jha, H. Wang, X.L. Phuah, H. Wang, T. Tsakalakos, Scripta Mater. 155 (2018) 37-40.
[22] J. Narayan, Scripta Mater. 69(2) (2013) 107-111.
[23] K. Naik, S.K. Jha, R. Raj, Scripta Mater. 118 (2016) 1-4.
[24] H. Charalambous, S.K. Jha, K.H. Christian, R.T. Lay, T. Tsakalakos, J. Eur. Ceram. Soc. 38(10) (2018) 3689-3693.
[25] J.S.C. Francis, M. Cologna, R. Raj, J. Eur. Ceram. Soc. 32(12) (2012) 3129-3136.
[26] J.M. Lebrun, C.S. Hellberg, S.K. Jha, W.M. Kriven, A. Steveson, K.C. Seymour, N. Bernstein, S.C. Erwin, R. Raj, J. Am. Ceram. Soc. 100(11) (2017) 4965-4970.
[27] J.C. M'Peko, J.S.C. Francis, R. Raj, D. Lupascu, J. Am. Ceram. Soc. 96(12) (2013) 3760-3767.
[28] R. Muccillo, E.N.S. Muccillo, J. Eur. Ceram. Soc. 33(3) (2013) 515-520.
[29] J. Park, I.W. Chen, D. Clarke, J. Am. Ceram. Soc. 96(3) (2013) 697-700.

[30] D. Yadav, R. Raj, J. Am. Ceram. Soc. 100(12) (2017) 5374-5378.
[31] S.K. Jha, H. Charalambous, H. Wang, X.L. Phuah, C. Mead, J. Okasinski, H. Wang, T. Tsakalakos, Ceram. Int. 44(13) (2018) 15362-15369.
[32] L.A. Perez-Maqueda, E. Gil-Gonzalez, A. Perejon, J.-M. Lebrun, P.E. Sanchez-Jimenez, R. Raj, J. Am. Ceram. Soc. 100(8) (2017) 3365–3369.
[33] E. Gil-Gonzalez, A. Perejon, P.E. Sanchez-Jimenez, M.J. Sayagues, R. Raj, L.A. Perez-Maqueda, J. Mater. Chem. A (2018).
[34] A. Perejón, N. Masó, A.R. West, P.E. Sánchez-Jiménez, R. Poyato, J.M. Criado, L.A. Pérez-Maqueda, J. Am. Ceram. Soc. 96(4) (2013) 1220-1227.
[35] S. Nandy, P.S.V. Mocherla, C. Sudakar, J. Appl. Phys. 121(20) (2017) 203102.
[36] L.C. Wang, Z.H. Wang, S.L. He, X. Li, P.T. Lin, J.R. Sun, B.G. Shen, Physica B 407(8) (2012) 1196-1202.
[37] A. Perejón, N. Murafa, P.E. Sánchez-Jiménez, J.M. Criado, J. Subrt, M.J. Diánez, L.A. Pérez-Maqueda, J. Mater. Chem. C 1(22) (2013) 3551.
[38] I. Sosnowska, R. Przeniosło, P. Fischer, V.A. Murashov, J. Magn. Magn. Mater. 160 (1996) 384-385.
[39] M. Wojdyr, J. Appl. Crystallogr. 43(5 Part 1) (2010) 1126-1128.
[40] S.K. Jha, J.M. Lebrun, K.C. Seymour, W.M. Kriven, R. Raj, J. Eur. Ceram. Soc. 36(1) (2016) 257-261.

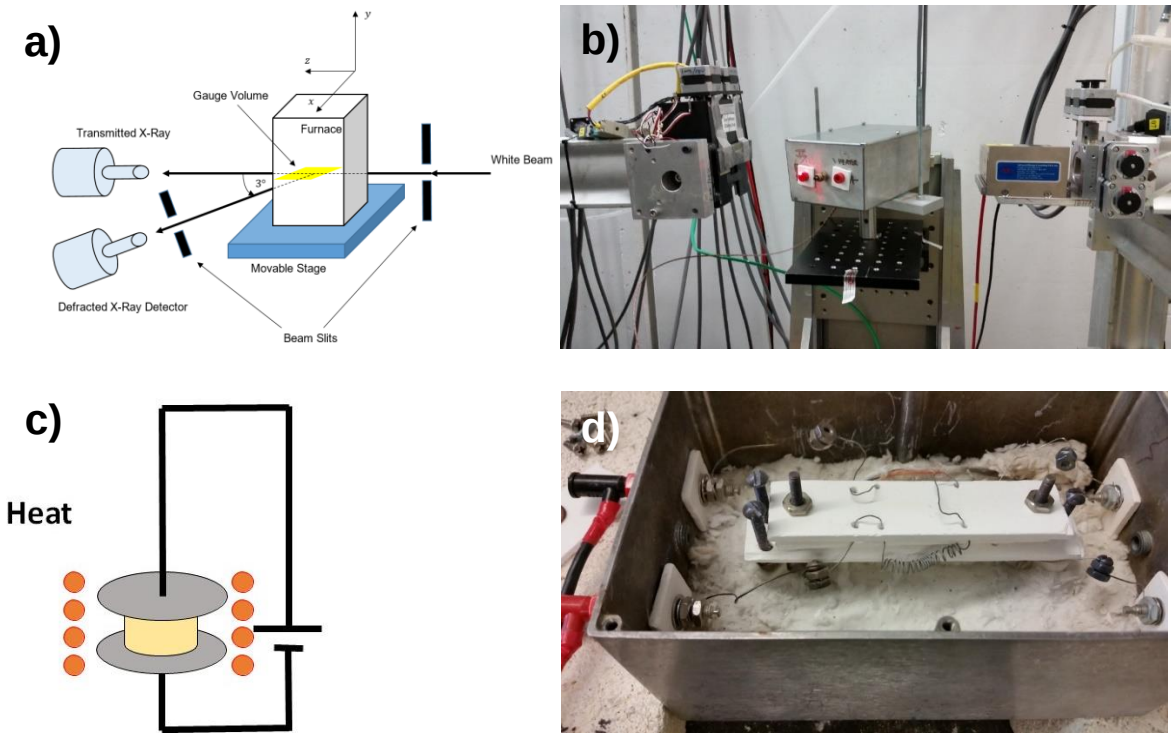

Figure 1: Schematic of 6-BM-A beamline at APS (a). Photograph of beamline (b). Schematic of sample (c). Photograph of furnace interior with modified heating coils (d).

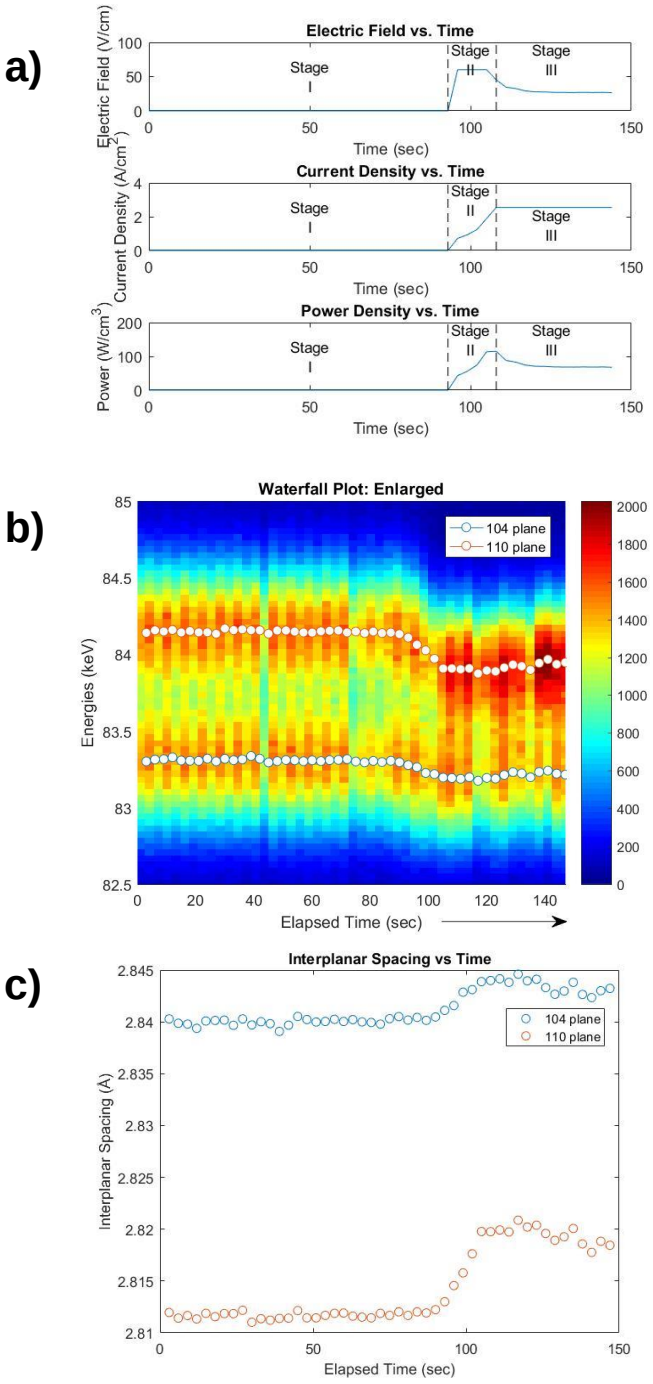

Figure 2: Electric field, current density, and power density versus time (a), peak energies versus time (b), interplanar spacing versus time during flash sintering of $BiFeO_3$ (c).

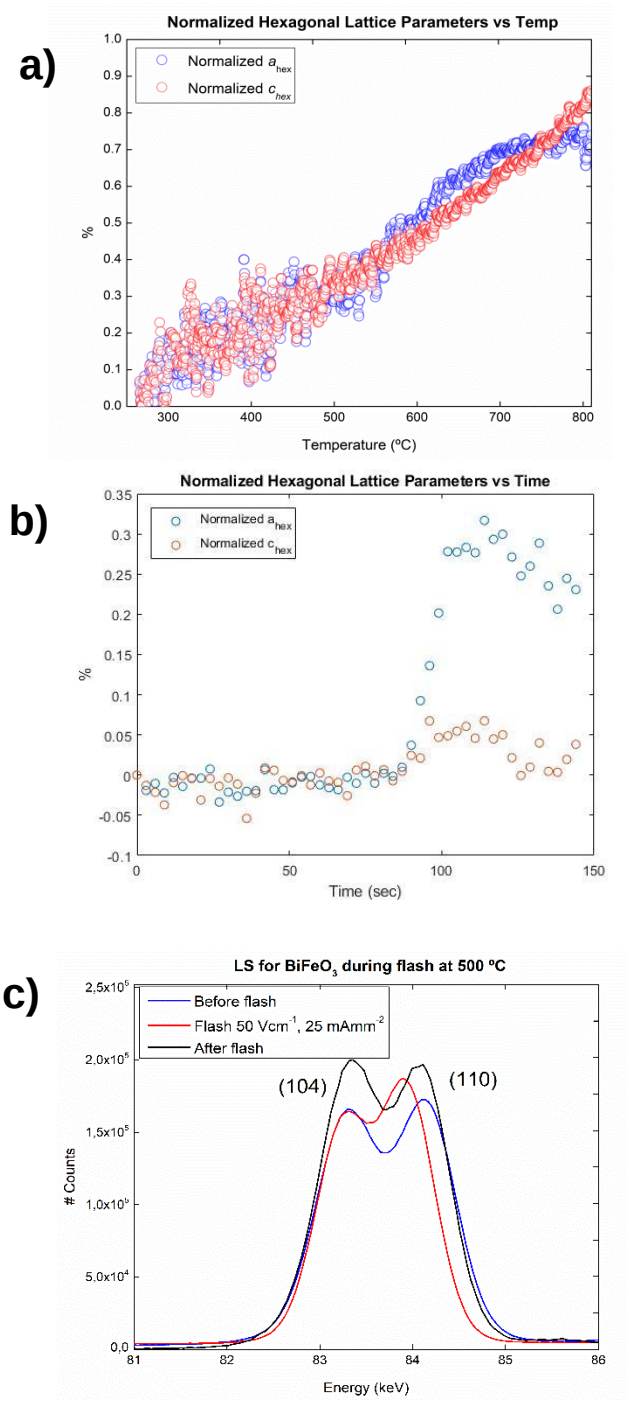

Figure 3: Normalized hexagonal lattice parameters calculated for a conventional temperature ramp-up with no applied electric field (a), normalized hexagonal lattice parameters calculated for a flash sintering experiment (50 Vcm^{-1}, 25 $mAmm^{-2}$) at a furnace temperature of 500°C (b), change in energy during flash for the diffraction peaks corresponding to the (104) and (110) planes (c).

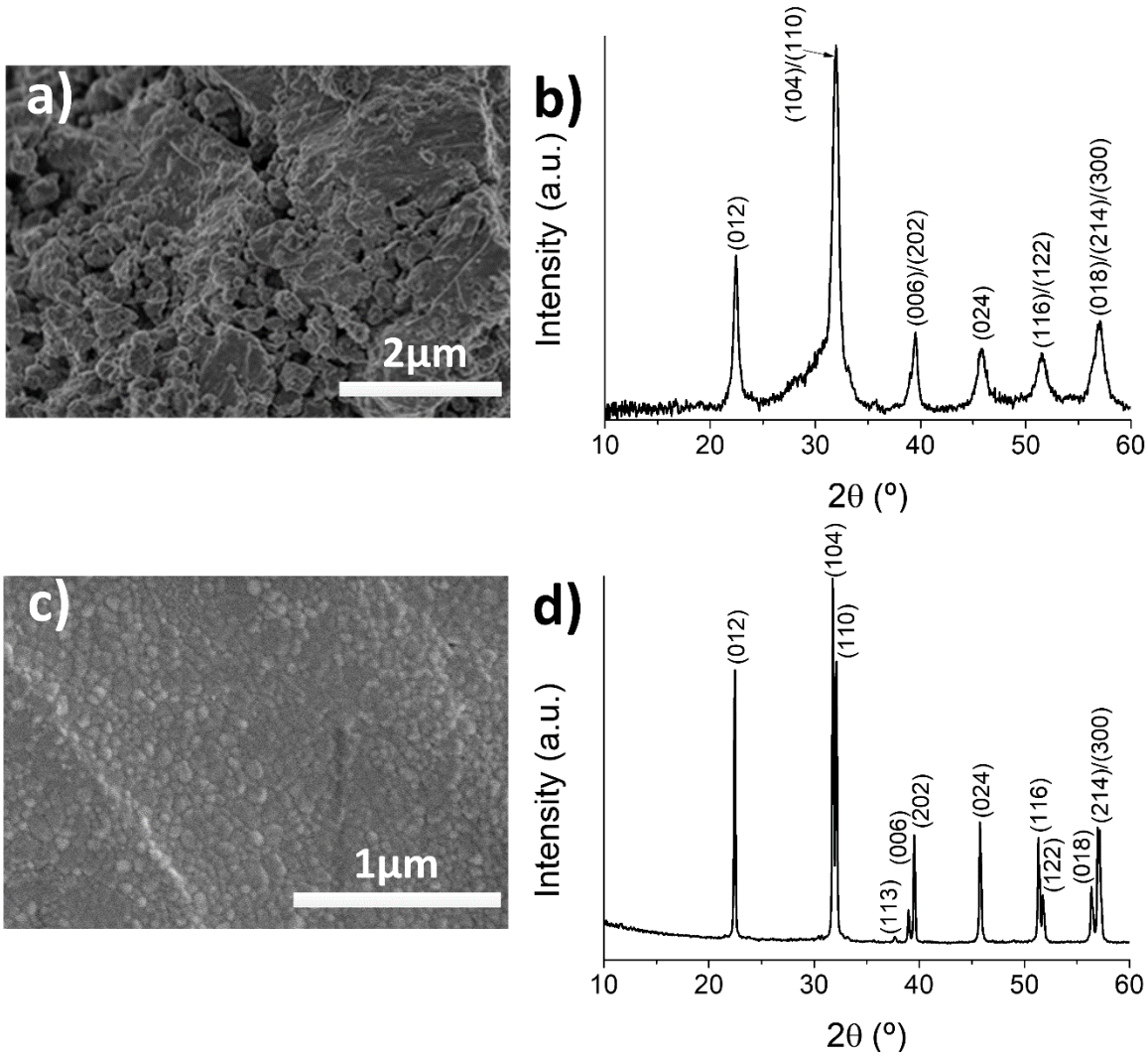

Figure 4: An indication of densification: SEM micrograph of mechanosynthesized $BiFeO_3$ powder (a), XRD pattern of the mechanosynthesized sample (b) SEM micrograph of $BiFeO_3$ densified by flash sintering at a furnace temperature of 500°C (c), and XRD pattern of the flash sintered sample (d).